Heliyon 9 (2023) e18006

Contents lists available at ScienceDirect

Heliyon

journal homepage: www.cell.com/heliyon

Morphological characteristics of astrocytes of the fastigial nucleus

Marianne Lizeth Martínez-Mendoza [a], Cynthia Alejandra Rodríguez-Arzate [a], Gabriela B. Gómez-González [a], Abraham Rosas-Arellano [b], Ataúlfo Martínez-Torres [a,*]

[a] Instituto de Neurobiología, Universidad Nacional Autónoma de México, Departamento de Neurobiología Celular y Molecular, Laboratorio de Neurobiología Molecular y Celular, Juriquilla, Querétaro, 76230, Mexico
[b] Unidad de Imagenología, Instituto de Fisiología Celular, Universidad Nacional Autónoma de México, 04510. Ciudad de México, Mexico

ARTICLE INFO

Keywords:
Cerebellum
Deep cerebellar nuclei
GFAP

ABSTRACT

Astrocytes are a diverse and morphologically complex class of glial cells restricted to the central nervous system which have been implicated in the modulation of neuronal activity. The cerebellum is involved in planning movements and motor learning. Within the cerebellum three deep cerebellar nuclei (dentate, interposed and fastigial) provide the sole neuronal output. The fastigial nucleus participates in saccadic and vestibular function, and recent evidence disclosed neuronal projections to cognitive, affective, and motor areas. However, thus far there are no reliable descriptions of the distribution and morphological classifications of astrocytes in this nucleus. This work aims to describe the characteristics of astrocytes of the fastigial nucleus based on the expression of GFP in a transgenic mouse model.

1. Introduction

The cerebellum is a structure of the hindbrain which coordinates voluntary movement, but it is also involved in cognitive and linguistic tasks and emotional and perceptual processing [1–3]. In the cerebellum, the grey matter is tightly folded forming the cerebellar cortex which in turn is divided into three layers: the molecular, the Purkinje, and the granular layer. The deep cerebellar nuclei (DCN) are embedded in the white matter beneath the cerebellar cortex at the roof of the fourth ventricle. The DCN are the dentate nucleus, the interposed nucleus, and the fastigial nucleus (FN). These nuclei form the only output pathway of the cerebellum [4].

The FN (also known as medial nucleus) receives GABAergic input from the cerebellar vermis and flocculus and glutamatergic input from the nucleus reticularis tegmenti pontis, the medial vestibular nucleus, the inferior olive and the medullary reticular formation. Neurons of the FN project to over sixty regions including the spinal cord, cerebellar cortex, thalamus, and medulla oblongata [5–7]. Besides its function in motor coordination, there is evidence of its role in non-somatic functions, such as cardiovascular, feeding, and respiratory activities [8–10]. Ablation of the FN attenuates the respiratory response to hypercapnia and hypoxia [11] and researchers have proposed the existence of respiratory-modulated neurons that do not show respiratory-related phasic activity until exposed to hypercapnia. Thus, like the ventrolateral medulla of the brainstem [12], the FN may be considered a central respiratory chemoreceptor.

* Corresponding author. Universidad Nacional Autónoma de México, Departamento de Neurobiología Celular y Molecular, Laboratorio de Neurobiología Molecular y Celular, Juriquilla, Querétaro, 76230, Mexico.
E-mail address: ataulfo@unam.mx (A. Martínez-Torres).

https://doi.org/10.1016/j.heliyon.2023.e18006
Received 18 October 2022; Received in revised form 8 May 2023; Accepted 5 July 2023
Available online 6 July 2023
2405-8440/© 2023 The Authors. Published by Elsevier Ltd. This is an open access article under the CC BY-NC-ND license (http://creativecommons.org/licenses/by-nc-nd/4.0/).

Although much attention has been paid to the role of neurons as the principal respiratory chemoreceptors, glial cells are endowed with molecular components that respond upon changes in extracellular pH such as inwardly rectifying potassium channels [13]. Astrocytes are depolarized by acidification, which induces the release of ATP. ATP release promotes the propagation of calcium waves that can travel hundreds of microns over a time scale of seconds modulating the activity of brain circuits and behavior [14,15]. Thus, the physiology of the FN may be affected by modifications in astrocyte intercommunication.

The FN presents a modular organization that consists of three regions (rostral, medial, and caudal) with a distinctive distribution of neuronal morphologies [16]. However, the distribution and morphology of astrocytes in the FN has not been documented and may be relevant to understanding FN in its role as a respiratory chemoreceptor and in its other functions. Here, we assess the distribution and morphological characteristics of astrocytes in the FN, and their relation to the vasculature.

2. Materials and methods

2.1. Animals

Experimental manipulations and protocols were performed in male mice at postnatal day 30 (P30), from the transgenic strain GFAP-eGFP [17]. Animals were housed and maintained in a temperature-controlled environment on a 12-h light–dark cycle, with *ad libitum* food and water. All procedures were conducted in accordance with the animal protocol (INEU/SA/CB089) for animal care and handling approved by the Bioethics committee of the Institute of Neurobiology of the Universidad Nacional Autónoma de México, as well as with national (NOM-062-ZOO-1999) and international guidelines (National Institutes of Health, USA).

2.2. Tissue processing

GFAP-eGFP mice postnatal day (P30) were anesthetized with pentobarbital, then transcardially perfused with saline solution (0.9%), followed by 4% paraformaldehyde (PFA) at pH 7.4, dissolved in phosphate-buffered saline (PBS). The brains (N = 5) were isolated and cryoprotected in sucrose (10 to 30%). Brains were sliced (30–40 μm thick) with a cryostat, from Bregma −6.84 mm to −5.88 mm. Slices were mounted in Superfrost®Plus/Colorfrost by Daigger and stored until their use. The cell nuclei were labeled with 4′,6-diamidino-2-phenylindole (DAPI, N = 4). For blood vessel labeling, Dil carbocyanine was used in GFAP-eGFP mice (N = 4), according to Li Y et al. (2008), [18]. The perfusion with this solution stained endothelial cells lining blood vessels.

2.3. Epifluorescence and confocal microscopy

Confocal and epifluorescence images were obtained with a Zeiss confocal microscope (LSM 780) and an Axio Scan.Z1 fluorescence microscope respectively. The resolution for each image was 1024 × 1024 pixels. Z-stack images and quantitative analysis were processed using ImageJ analysis software. The diode lasers used were Argon, excitation wavelength 488 nm and emission 517 nm, DPSS 561 nm to 618 nm and laser 405 nm with an emission of 465 nm. Emission filters were used to detect GFP-YFP/FG, FR/Alexa 594, and DAPI respectively. The objectives used were 10x/0.45, 20x/0.8, 40x/1.30 Oil DIC and 63x/1.40 Oil DIC. A Zeiss Axioscope 2 epifluorescence microscope was used for low magnification images of the FN.

2.4. Morphometric analysis

In all images a resolution of 1024 × 1024 pixels with a size of 0.21 μm x pixel was obtained with an EC plan-Neofluar 40x/1.30 Oil DIC M27 objective, with a depth of 8 BIT. 30–40 μm brain slices (N = 4) were analyzed and astrocytes were randomly selected from the FN. 15 astrocytes per brain were analyzed.

The following inclusion criteria were used for cell reconstructions: 1) The astrocytes should have presented a single, isolated nucleus and fully reconstructed in z-focal planes, 2) must had to have uninterrupted processes extending from the cell body and the majority of the processes intact. Several images taken at different focal depths (z-stack) were obtained and analyzed through individual stacks when it was necessary to distinguish between processes that overlapped in the maximum projection. Therefore, cells in which the processes could not be clearly observed in each focal plane were not included in this analysis.

Z-stack projections of confocal sections were pre-processed using an automated macro in Fiji-ImageJ software. For each cell, maximum projection images were converted into binary images. Thresholds were set to label the cell body and processes, avoiding background pixels. To determine the number of intersections, length of processes and ramification index, the analysis was carried out using the Sholl Analysis plugin of ImageJ v.140 [19–21]. Sholl analysis was performed with concentric circles using 10 μm radius steps and the maximal ring was determined by the intersection of the rings with the longest processes. The complexity of astrocyte processes from different regions was assessed by determining the ramification index, using the ratio between critical value of the adjusted profile and the maximum intersection number of primary branches [20].

2.5. Fastigial nucleus vasculature

VasoMetrics, a macro written in Fiji-ImageJ for spatiotemporal analysis of microvasculature [22], was used to determine the length and diameter of blood vessels. Image stacks of DiI-labeled vessels of GFAP-eGFP mice were selected from the three regions of the FN and reconstructed in VasoMetrics (n = 8 to 10 vessels per section, three sections for each region at P30).

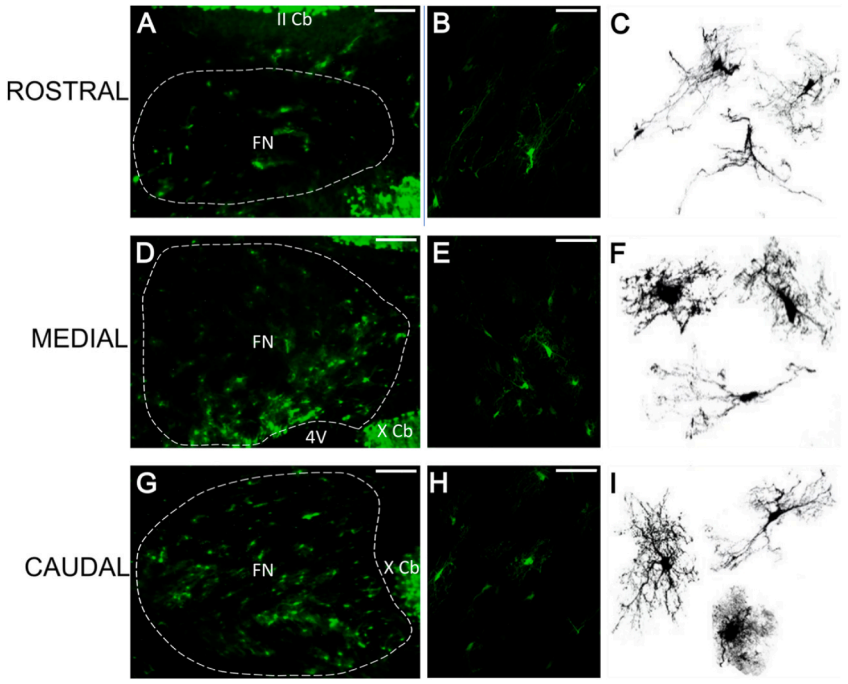

Fig. 1. Astrocytes in the fastigial nucleus of the GFAP-eGFP transgenic mouse. The FN was sectioned in coronal sections and divided in three regions. Low magnification epifluorescence images of the rostral **(A)**, medial **(D)** and caudal **(G)** regions showed a gradient of density from lower in the rostral section to the highest in the caudal. **B**, **E**, and **H**, high magnification confocal images showed the diversity of morphological characteristics of astrocytes in the three regions. In the rostral region many processes project to the ventral area (scale bar 50 μm). **C**, **F**, and **I** show images of astrocytes sampled in different sections of the three regions. Scale bar in A, D, and G 100 μm.

2.6. Statistical analysis

For statistical analysis, data sets were tested with Shapiro–Wilk or Kolmogorov–Smirnov for normality. The density of astrocytes in each fastigial region (rostral, medial, and caudal) was compared applying Kruskal–Wallis ANOVA followed by Dunn's post hoc test. Data from cell's soma area, diameter and Sholl analysis were analyzed by one-way ANOVA followed by Bonferroni's comparison test. To determine the length of vasculature in each fastigial region data were analyzed applying Kruskal-Wallis ANOVA followed by Dunn's post hoc test. For blood vessel diameters, one-way ANOVA was used followed by Bonferroni's comparison test. All data are represented as mean ± SEM and data marked with asterisks are significantly different from the control as follows: ***$p < 0.001$, **$p < 0.01$, and *$p < 0.05$.

3. Results

3.1. Astrocyte density and morphology

The characterization of diverse astrocyte populations in the three regions of the mouse FN was based on the analysis of optical sections (z-stack depth 40 μm) obtained by confocal microscopy (LSM 780 ZEISS, 40X) and divided into rostral, caudal, and medial regions as previously published [16,23].

The density of astrocytes present in each fastigial region was estimated by counting the number of astrocytes (GFAP-eGFP positive) in an area of 1 mm^2 per coronal section; three sections for each region ($n = 15$). These showed differences in the density of astrocytes in each region, the caudal region had the highest density (281.47 astrocytes/mm^2), followed by the medial region (211.76 astrocytes/mm^2), finally the rostral region had the lowest density (91.18 astrocytes/mm^2). Sample low-magnification images are shown in Fig. 1A, D and G, where the scattered distribution of GFP + cells is observed in the rostral region compared to the medial and caudal regions. Fig. 1B, E and H show examples of high magnification (20x objective) of astrocytes in each region of the FN. In the rostral region many astrocytic processes project ventrally; however, this array was not found in the medial and caudal regions. For morphological analysis, images were converted into binary format to show the fine distal processes of the astrocytes. A collection of astrocytes from the three regions is shown in Fig. 1C, F and I, where at least two different morphologies were identified as described below.

Sholl analysis of reconstructed astrocytes from the FN was performed with the Sholl plugin from Fiji-ImageJ software with concentric circles of 10 μm radius steps from the center of the soma (Fig. 2A–C). The maximal ring was determined by the intersection of the rings with the longest processes, where the average number of intersections was lower in the rostral region (5.22 ± 1.70, $n = 15$)

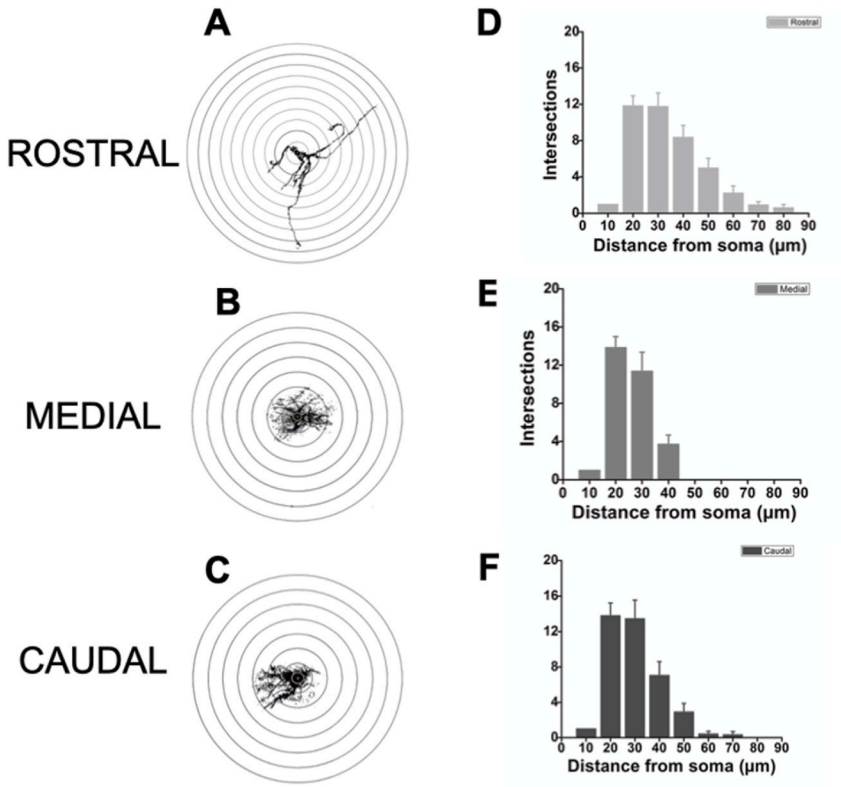

Fig. 2. Morphometric analysis of FN astrocytes. A-C. Representative Sholl analysis from the three regions of the FN, the data analyzed were from 15 cells per region, in adult male mice GFAP-eGFP, postnatal day 30. **D-F**. Distance from soma in incremental spaces of 10 μm in astrocytes with the numbers of process intersections from each region.

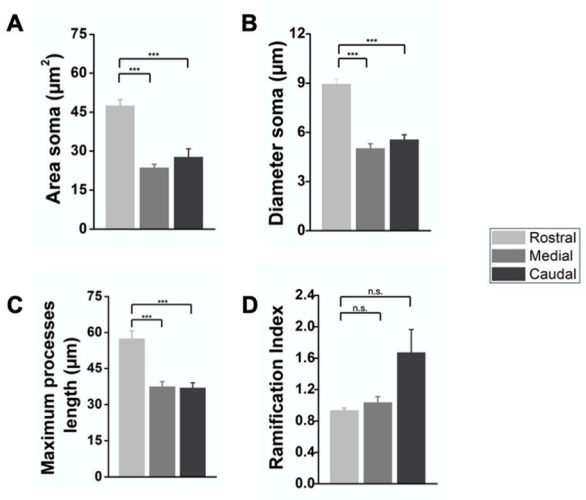

Fig. 3. Morphometric features. Summary of data analysis. **A-B**. Area and diameter from somas. **C**. Maximum length of processes. **D**. Ramification index. Error bars SEM, n = 15 cells per region, in male mice GFAP-GFP, P30.

compared with caudal (7.65 ± 2.63, n = 15, p = 0.71) and medial regions (7.5 ± 3.05, n = 15, p = 0.77), which did not show significant differences (Fig. 2D–F).

Quantitative analyses of area, diameter, maximum length process, average number of process intersections and ramification index were determined from the three regions. Area and diameter of the somas showed statistical differences between the rostral-caudal and rostral-medial regions (one-way ANOVA, Bonferroni's post hoc test). Somas of the rostral region were the largest (area: 47.47 ± 2.35

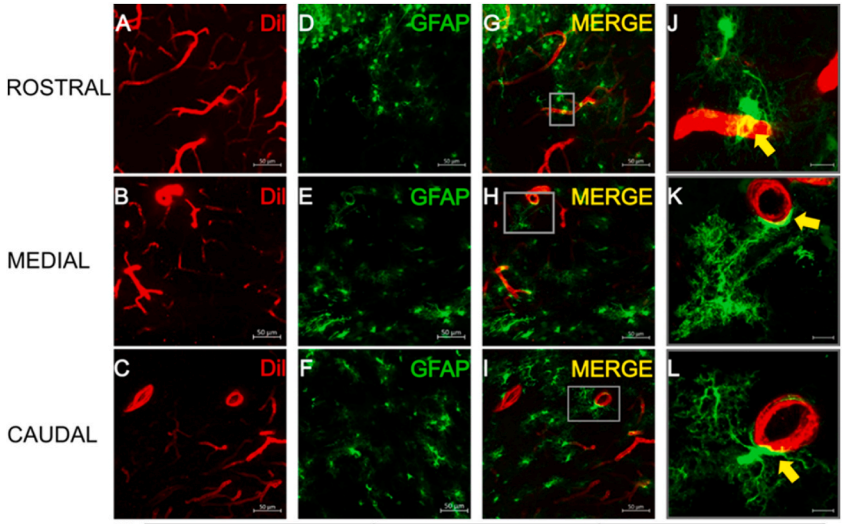

M

Fastigial region	Diameter (μm)	Length (μm)
Rostral	5.95 ± 0.20	140.67 ± 14.92
Medial	5.94 ± 0.28	88.93 ± 8.33
Caudal	6.00 ± 0.29	106.05 ± 7.42

Fig. 4. Vasculature in the FN. A-C. DiI labeling of blood vessels did not reveal differences in distribution, diameter, and length. **G**, **H**, and **I**. Similar to other brain areas astrocytes make extensive contacts with the vasculature. **J**, **K**, and **L** High magnification images revealed astrocytes in intimate contact with blood vessels in the three regions of the FN (yellow arrows). **M**. Comparative analysis of blood vessel diameter and length in the three regions of the FN. N = 4 in GFAP-GFP male mice P30, blood vessels n = 10 per region. (A–I) scale bar 50 μm and J-L 10 μm. (For interpretation of the references to colour in this figure legend, the reader is referred to the Web version of this article.)

μm^2, n = 15; diameter: 8.93 ± 0.30 μm, n = 15), while somas of the caudal (area: 27.64 ± 3.24 μm^2, n = 15, $p < 0.001$; diameter: 5.54 ± 0.30 μm, n = 15, $p < 0.001$) and medial regions (area: 23.54 ± 1.39 μm^2, n = 15, $p < 0.001$; diameter: 5.01 ± 0.28 μm, n = 15, $p < 0.001$) were similar (Fig. 3A–B). Thus, in the rostral region there were fewer astrocytes, but with larger somas. Astrocyte processes of the rostral region (57.34 ± 3.37 μm, n = 15) were larger than those of the caudal (36.92 ± 2.15 μm, n = 15, p = 0.0001) and the medial regions (37.40 ± 2.08 μm, n = 15, p = 0.0001) (Fig. 3C). The ramification index of astrocytes in the caudal region (1.67 + 0.29, n = 10, p = 0.26) seemed higher compared to the medial (1.03 + 0.07, n = 10, p = 0.39) and rostral (0.93 + 0.03, n = 10, p = 0.38) regions but did not show significant differences (Fig. 3D). These results showed that astrocytic processes from medial and caudal fastigial regions are more densely arranged with multiple processes distributed homogeneously around the soma, similar to velate astrocytes; in contrast to the processes of the rostral region, where astrocytes present less morphological complexity with longer and less branched processes.

3.2. Blood vessels

Astrocyte somas are usually well spaced from one another, and blood vessels often appear to have an influence on the organization of astrocytic processes and on overall astrocyte morphology [24]. Therefore, it is relevant to understand the organization of astrocytes in the context of vasculature.

Sample images of DiI-labeled blood vessels in the three regions of the FN are shown in Fig. 4A, B and C. Visual inspection of the distribution and arrangement of the vasculature did not reveal marked differences between regions, which was confirmed quantitatively. First, the average vessel length did not exhibit significant differences in the caudal (106.05 ± 7.42 μm^2, n = 3, p = 0.45), medial (88.93 ± 8.33 μm^2, n = 3) and rostral (140.67 ± 14.92 μm^2, n = 3) regions; second, the vessel diameter was similar in the three regions: caudal (6.00 ± 0.29 μm, n = 8, p = 0.95), medial (5.94 ± 0.28 μm, n = 8, p = 0.98) and rostral (5.95 ± 0.20 μm, n = 8, p = 0.99) (Fig. 4M). The number of blood vessel segments was similar in the three regions in an area of 1 mm^2: rostral (85.7, n = 3), medial (72.9, n = 3), and caudal (95.3 n = 3). This finding was unexpected since astrocyte density in the rostral region is low, as shown in the previous section. Thus, differences in astrocytic density and morphological complexity between regions of the FN are not influenced by the arrangement of blood vessel segments or by the length or diameter of the vasculature from each region. Nonetheless, astrocytes make extensive contacts with the FN vasculature (Fig. 4J, K and L), similar to astrocytes from other brain areas.

3.3. Relation with cerebrospinal fluid

Finally, we inspected the interface between the fourth ventricle and the subventricular zone proximal to the FN to assess whether

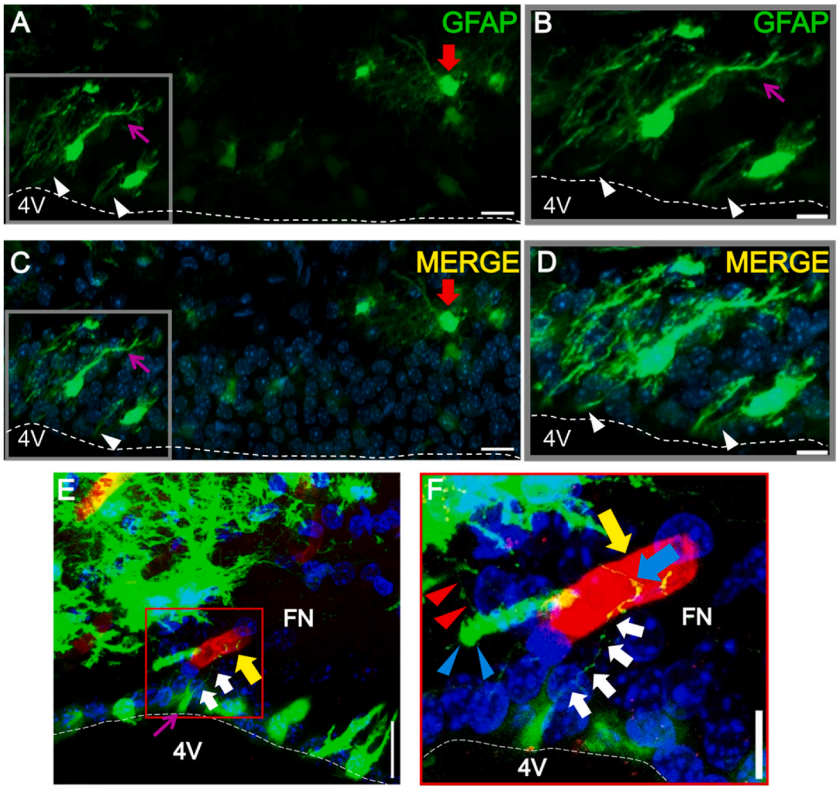

Fig. 5. Subventricular cells in contact with the CSF and FN. A and **C.** Along the wall of the fourth ventricle at the level of the medial region of the FN, some GFAP + cells (ependymal cells) show their soma in the subventricular zone and project a long process toward the FN (purple arrow) and multiple short processes to the light of the ventricle (white arrowheads). A protoplasmic astrocyte within the FN is indicated by a red arrow. Cell nuclei stained with DAPI. **B** and **D.** High magnification images of the grey box in A and C. The discontinuous lines indicate the edge of the fourth ventricle. Scale bar in A and C, 20 μm, B and D, 10 μm. In **E** and **F,** cell processes (white arrows) that are directed towards the blood vessels (yellow arrow) and the contact between them (blue arrow). GFAP-eGFP positive cells (blue arrowheads) with the processes towards the medial part of the FN (red arrowheads) and the soma very close to the blood vessel. Scale bar E (20 μm) and F (10 μm). (For interpretation of the references to colour in this figure legend, the reader is referred to the Web version of this article.)

GFP + cells in the area could contact the cerebrospinal fluid (CSF) and the FN (Fig. 5). This could provide evidence that astrocytes or other glial cells can gate biochemical signals from the CSF to the FN. We found intermingled between ependymal glial cells of the wall of the fourth ventricle a population of GFP + cells whose soma is in the subventricular zone with short processes that project to the lumen of the ventricle and a single long process with short ramifications that project to the FN. These cells were found only in the medial region of the FN and some examples are shown in Fig. 5A–D. Furthermore, some of these cells contacted both the CSF and blood vessels of the FN as shown in Fig. 5E–F.

4. Discussion

By employing a combination of transgenic mice and confocal microscopy we have identified the morphological characteristics of astrocytes in the mature FN of the mice cerebellum. Astrocytes are the most abundant glial cell in the brain, where they provide support to neurons and regulate synaptic transmission and plasticity. However, their morphological heterogeneity and how it is related to their multiple functional roles has not been revealed in the FN. Our findings show the morphological diversity of astrocytes and their distribution in three discrete regions of the FN.

The GFAP-eGFP transgenic mouse line facilitated the identification of astrocytes in the FN and the inspection of their distribution and morphological characteristics. The morphology of astrocytes and its response to diverse stimuli have been assessed in this mouse strain [25–29]. Because GFP is widely distributed in this transgenic strain, the astrocyte morphology can be characterized on different levels: from the number of main branches to the array of their small processes. In contrast, GFAP immunolabeling is predominantly distributed in the main branches and perinuclear region of the astrocytes. However, a potential caveat in using the transgenic model is that it may not report all the astrocytes in several brain areas, but it is known that in the cerebellum GFP expression driven by the hGFAP promoter highly correlates with GFAP immunolabeling in the mouse strain used in our study which has an FVB genetic background [17,30].

We divided the FN into rostral, medial, and caudal regions according to previous reports [16,23]. Astrocytes exhibit a gradient of

density, which is lowest in the rostral region and highest in the caudal region. Previous studies have noted the anatomical division of the FN in terms of neuronal distribution. Voogd et al. (2013) [31], divided the FN into three regions according to the distribution of a retrograde neural tracer injected into the contralateral FN, whereas Beitz and Chan-Palay (1979) divided the FN into three regions according to neuron morphology revealed by silver impregnation [16]. We found that in coronal sections of the FN, astrocytes are also distributed in three discrete regions similar to those proposed by the latter authors. Furthermore, the astrocytes of the FN organize into modular domains in the three regions. Astrocyte processes residing within the caudal and medial regions appear to occupy overlapping spatial domains, where they are densely intermingled. In contrast, rostral astrocytes appear to occupy distinct spatial domains, establishing exclusive territories in the same way as astrocytes in the hippocampus and cortex [32–34].

Understanding the anatomical association between astrocytes and brain vasculature is central for deciphering the regulation of cerebral blood flow. We did not find literature on the organization of blood vessels in the FN and considered that studying this matter in the context of astrocyte diversity was important. We predicted that blood vessel distribution would be divided into separate regions such as neurons and astrocytes [16,31]; however, this was not the case. The average vessel length and diameter was similar in the three regions of the FN, and we did not find a relationship between the distribution of astrocyte morphologies and arrangement of blood vessel.

The ependymal layer forms a semi-permeable barrier that modulates the exchange of biochemical signals between the CSF and brain parenchyma. In mice, astrocytes are interposed within the ependymal layer in neurogenic niches [35,36]. Strikingly, we noticed that the processes of many ependymal cells neighboring the FN medial region reach the lumen of the fourth ventricle and make contact with the CSF and blood vessels (Fig. 5). Whether these cells gate signals from the CSF to the FN or blood vessels will be further investigated.

Author contribution statement

Marianne Lizeth Martínez-Mendoza, Cynthia Alejandra Rodríguez-Arzate, Ataúlfo Martínez-Torres: Conceived and designed the experiments; Performed the experiments; Analyzed and interpreted the data; Contributed materials, analysis tools; Wrote the paper.

Gabriela B. Gómez-González, Abraham Rosas-Arellano: Conceived and designed the experiments; Contributed materials, analysis tools; Wrote the paper.

Data availability statement

Data will be made available on request.

Declaration of competing interest

The authors declare that they have no known competing financial interests or personal relationships that could have appeared to influence the work reported in this paper.

Acknowledgments

This work was supported by grants from CONACYT (A1S7659) and UNAM-DGAPA-PAPIIT (IN204520). MLMM was supported by fellowships from CONACYT (597956) and from PAPIIT-DGAPA-UNAM (Fellowship 597956). Jessica González Norris kindly edited the manuscript. Prof. H. Kettenmann (MDC-Berlin) and Dr. Reyes-Haro (INB-UNAM) donated the transgenic mouse line hGFAP-eGFP. We thank technical support of Dr. A. E. Espino-Saldaña, Dr. R. Arellano's laboratory, the INB-UNAM vivarium (M. García Servin, A. Castilla-Leon, M. A. Carbajo) and INB-UNAM microscopy facility (E.N. Hernández).

References

[1] M. Ito, Cerebellar circuitry as a neuronal machine, Prog. Neurobiol. 78 (2006) 272–303, https://doi.org/10.1016/j.pneurobio.2006.02.006. PMID: 16759785.
[2] L.F. Koziol, D. Budding, N. Andreasen, S. D'Arrigo, S. Bulgheroni, H. Imamizu, M. Ito, M. Manto, C. Marvel, K. Parker, G. Pezzulo, N. Ramnani, D. Riva, J. Schmahmann, L. Vandervert, T. Yamazaki, Consensus paper: the cerebellum's role in movement and cognition, Cerebellum 1 (2014) 151–177, https://doi.org/10.1007/s12311-013-0511-x.
[3] J.D. Schmahmann, An emerging concept. The cerebellar contribution to higher function, Arch. Neurol. 48 (1991) 1178–1187, https://doi.org/10.1001/archneur.1991.00530230086029.
[4] J. Voogd, M. Glickstein, The anatomy of the cerebellum, Trends Neurosci. 9 (1998) 370–375.
[5] M.W. Bagnall, B. Zingg, A. Sakatos, S.H. Moghadam, H. U Zeilhofer, S. du Lac, Glycinergic projection neurons of the cerebellum, J. Neurosci. 29 (2009), https://doi.org/10.1523/JNEUROSCI.2087-09.2009, 10104-0110.
[6] H. Fujita, T. Kodam, S. du Lac, Modular output circuits of the fastigial nucleus for diverse motor and nonmotor functions of the cerebellar vermis, Elife (2020), https://doi.org/10.7554/eLife.58613.
[7] T.J. Ruigrok, J. Voogd, Cerebellar nucleo-olivary projections in the rat: an anterograde tracing study with Phaseolus vulgaris-leucoagglutinin (PHA-L), J. Comp. Neurol. 298 (1990) 315–333, https://doi.org/10.1002/cne.902980305.
[8] S.K. Manchanda, O.P. Tandon, I.S. Aneja, Role of the cerebellum in the control of gastro-intestinal motility, J. Neural. Transm. 33 (1972) 195–209, https://doi.org/10.1007/BF01245317.
[9] J.N. Zhu, W.H. Yung, B. Kwok-Chong Chow, Y.S. Chan, J.J. Wang, The cerebellar-hypothalamic circuits: potential pathways underlying cerebellar involvement in somatic-visceral integration, Brain Res. Rev. 52 (2006) 93–106, https://doi.org/10.1016/j.brainresrev.2006.01.003.
[10] J.N. Zhu, J.J. Wang, The cerebellum in feeding control: possible function and mechanism, Cell. Mol. Neurobiol. 28 (2008) 469–478, 10. 1007/s10571-007-9236-z.

[11] F. Xu, D.T. Frazier, Role of the cerebellar deep nuclei in respiratory modulation, Cerebellum 1 (2002) 35–40, https://doi.org/10.1080/147342202753203078.
[12] P.G. Guyenet, D.A. Bayliss, Central respiratory chemoreception, Handb. Clin. Neurol. 188 (2010) 37–72, https://doi.org/10.1016/B978-0-323-91534-2.00007-2.
[13] J. Weller, C. Steinhäuser, G. Seifert, pH-sensitive K(+) currents and properties of K2P channels in murine hippocampal astrocytes, Adv. Protein. Chem. Struct. Biol. 103 (2016) 263–294, https://doi.org/10.1016/bs.apcsb.2015.10.005.
[14] A.V. Gourine, E. Llaudet, N. Dale, K.M. Spyer, ATP is a mediator of chemosensory transduction in the central nervous system, Nature 436 (2005) 108–111, https://doi.org/10.1038/nature03690.
[15] R.T. Huckstepp, R. id Bihi, R. Eason, K.M. Spyer, N. Dicke, K. Willecke, N. Marina, A.V. Gourine, N. Dale, Connexin hemichannel-mediated CO2-dependent release of ATP in the medulla oblongata contributes to central respiratory chemosensitivity, J. Physiol. 588 (2010) 3901–3920, https://doi.org/10.1113/jphysiol.2010.192088.
[16] A.J. Beitz, V. Chan-Palay, A Golgi analysis of neuronal organization in the medial cerebellar nucleus of the rat, Neuroscience 4 (1979) 47–63, https://doi.org/10.1016/0306-4522(79)90217-3.
[17] C. Nolte, M. Matyash, T. Pivneva, C.G. Schipke, C. Ohlemeyer, U.K. Hanisch, F. Kirchhoff, H. Kettenmann, GFAP promoter-controlled EGFP-expressing transgenic mice: a tool to visualize astrocytes and astrogliosis in living brain tissue, Glia 33 (2001) 72–86.
[18] Y. Li, Y. Song, L. Zhao, G. Gaidosh, A.M. Laties, R. Wen, Direct labeling and visualization of blood vessels with lipophilic carbocyanine dye DiI, Nat. Protoc. 3 (2008) 1703–1708, https://doi.org/10.1038/nprot.2008.172.
[19] J. Schindelin, I. Arganda-Carreras, E. Frise, V. Kaynig, M. Longair, T. Pietzsch, S. Preibisch, C. Rueden, S. Saalfeld, B. Schmid, J.Y. Tinevez, D.J. White, V. Hartenstein, K. Eliceiri, P. Tomancak, A. Cardona, Fiji: an open-source platform for biological-image analysis, Nat. Methods 9 (2012) 676–682, https://doi.org/10.1038/nmeth.2019.
[20] T.A. Ferreira, A.V. Blackman, J. Oyrer, S. Jayabal, A.J. Chung, A.J. Watt, J.P. Sjöström, D.J. van Meyel, Neuronal morphometry directly from bitmap images, Nat. Methods 10 (2014) 982–984, https://doi.org/10.1038/nmeth.3125.
[21] A. Srinivasan, A. Srinivasan R.J. Ferland, AutoSholl allows for automation of Sholl analysis independent of user tracing, J. Neurosci. Methods (2020) 108529, https://doi.org/10.1016/j.jneumeth.2019.108529.
[22] K.P. McDowell, A. A Berthiaume, T. Tieu, D.A. Hartmann, A.Y. Shi VasoMetrics, Unbiased spatiotemporal analysis of microvascular diameter in multi-photon imaging applications. Quant. Imag. Med. Surg. 11 (2021) 969–982, https://doi.org/10.21037/qims-20-920.
[23] G.B. Gómez-González, A. Martínez-Torres, Inter-fastigial projections along the roof of the fourth ventricle, Brain Struct. Funct. 226 (2021) 901–917, https://doi.org/10.1007/s00429-021-02217-8.
[24] T. Chan-Ling, J. Stone, Factors determining the migration of astrocytes into the developing retina: migration does not depend on intact axons or patent vessels, J. Comp. Neurol. 303 (1991) 375–386, https://doi.org/10.1002/cne.903030304.
[25] N. Daschil, C. Humpel, Green-fluorescent Protein(+) astrocytes attach to beta-amyloid plaques in an alzheimer mouse model and are sensitive for clasmatodendrosis, Front. Aging Neurosci. (2016), https://doi.org/10.3389/fnagi.2016.00075.
[26] D. Minge, C. Domingos, P. Unichenko, C. Behringer, A. Pauletti, S. Anders, M.K. Herde, A. Delekate, P. Gulakova, S. Schoch, G.C. Petzold, C. Henneberger, Heterogeneity and development of fine astrocyte morphology captured by diffraction-limited microscopy, Front. Cell. Neurosci. (2021), https://doi.org/10.3389/fncel.2021.669280.
[27] A.D. Rivera, A.M. Butt, Astrocytes are direct cellular targets of lithium treatment: novel roles for lysyl oxidase and peroxisome-proliferator activated receptor-γ as astroglial targets of lithium, Transl. Psychiatry (2019) 211, https://doi.org/10.1038/s41398-019-0542-2.
[28] S.O. Rohr, T. Greiner, S. Joost, S. Amor, P.V. Valk, C. Schmitz, M. Kipp, Aquaporin-4 Expression during Toxic and Autoimmune Demyelination, Cells (2020) 2187, https://doi.org/10.3390/cells9102187.
[29] M.B. Soria-Ortiz, P. Reyes-Ortega, A. Martínez-Torres, D. Reyes-Haro, A functional signature in the developing cerebellum: evidence from a preclinical model of autism, Front. Cell Dev. Biol. (2021) 727079, https://doi.org/10.3389/fcell.2021.727079.
[30] X. Bai, A.S. Saab, W. Huang, I.K. Hoberg, F. Kirchhoff, A. Scheller, Genetic background affects human glial fibrillary acidic protein promoter activity, PLoS One 8 (2013), https://doi.org/10.1371/journal.pone.0066873.
[31] J. Voogd, Y. Shinoda, T.J.H. Ruigrok, I. Sugihara, Cerebellar nuclei and the inferior olivary nuclei: organization and connections, in: M. Manto, J. D. Schmahmann, F. Rossi, D.L. Gruol, N. Koibuchi (Eds.), Handbook of the Cerebellum and Cerebellar Disorders, Springer, Dordrecht, 2013, pp. 377–436, https://doi.org/10.1002/1096-9861(20001016)426:2<209::aid-cne4>3.0.co;2-0.
[32] E.A. Bushong, M.E. Martone, Y.Z. Jones, M.H. Ellisman, Protoplasmic astrocytes in CA1 stratum radiatum occupy separate anatomical domains, J. Neurosci. 22 (2002) 83–92, https://doi.org/10.1523/JNEUROSCI.22-01-00183.2002.
[33] E.A. Bushong, M.E. Martone, Y.Z. Jones, M.H. Ellisman, Examination of the relationship between astrocyte morphology and laminar boundaries in the molecular layer of adult dentate gyrus, J. Comp. Neurol. 462 (2003) 241–251, https://doi.org/10.1002/cne.10728.
[34] M.M. Halassa, T. Fellin, H. Takano, J.H. Dong, P.G. Haydon, Synaptic islands defined by the territory of a single astrocyte, J. Neurosci. 27 (2007) 6473–6477, https://doi.org/10.1523/JNEUROSCI.1419-07.2007.
[35] J. Luo, S.B. Daniels, J.B. Lennington, R.Q. Notti, J.C. Conover, The aging neurogenic subventricular zone, Aging Cell 2 (2006) 139–152, https://doi.org/10.1111/j.1474-9726.2006.00197.x.
[36] J. Luo, B.A. Shook, S.B. Daniels, J.C. Conover, Subventricular zone-mediated ependyma repair in the adult mammalian brain, J. Neurosci. 14 (2008) 3804–3813, https://doi.org/10.1523/JNEUROSCI.0224-08.2008.